

1 **Size distribution and source of black carbon aerosol in**
2 **urban Beijing during winter haze episodes**

3 Yunfei Wu^{1,*}, Xiaojia Wang¹, Jun Tao², Rujin Huang³, Ping Tian⁴, Junji Cao³, Leiming
4 Zhang⁵, Kin-Fai Ho⁶, Zhiwei Han¹, Renjian Zhang^{1,*}

5
6 1 CAS Key Laboratory of Regional Climate-Environment for Temperate East Asia,
7 Institute of Atmospheric Physics, Chinese Academy of Sciences, Beijing, China

8 2 South China Institute of Environmental Sciences, Ministry of Environmental
9 Protection, Guangzhou, China

10 3 CAS Key Laboratory of Aerosol Chemistry and Physics, Institute of Earth
11 Environment, Chinese Academy of Sciences, Xi'an, China

12 4 Beijing Weather Modification Office, Beijing, China

13 5 Air Quality Research Division, Science and Technology Branch, Environment and
14 Climate Change Canada, Toronto, Canada

15 6 The Jockey Club School of Public Health and Primary Care, The Chinese
16 University of Hong Kong, Hong Kong, China

17
18 * Correspondence to: Yunfei Wu (wuyf@mail.iap.ac.cn) and Renjian Zhang (zrj@mail.iap.ac.cn)

19

20 **Abstract**

21 Black carbon (BC) has important impact on climate and environment due to its
22 light absorption ability, which greatly depends on its physicochemical properties
23 including morphology, size and mixing state. The size distribution of the refractory BC
24 (rBC) was investigated in urban Beijing during the late winter of 2014 with frequent
25 haze events, through analysis of measurements obtained using a single particle soot
26 photometer (SP2). By assuming void-free rBC with a density of 1.8 g cm^{-3} , the mass of
27 the rBC showed an approximately lognormal distribution as a function of the volume-
28 equivalent diameter (*VED*), with a peak diameter of 213 nm. Larger *VED* values of the
29 rBC were observed during polluted periods than clean days, implying an alteration in
30 the rBC sources, as the size distribution of the rBC from a certain source was relative
31 stable and *VED* of an individual rBC varied little once it was emitted into the
32 atmosphere. The potential source contribution function analysis showed that air masses
33 from the south to east of the observation site brought higher rBC loadings with more
34 thick coatings and larger core sizes. The mean *VED* of the rBC presented a significant
35 linear correlation with the number fraction of thickly coated rBC, extrapolating to be
36 $\sim 150 \text{ nm}$ for the completely thinly/non coated rBC. It was considered as the typical
37 mean *VED* of the rBC from local traffic sources in this study. Local traffic was
38 estimated to contribute 35% to 100% of the hourly rBC mass concentration with a mean
39 of 59% during the campaign. Lower local traffic contributions were observed during
40 polluted periods, suggesting increasing contributions of other sources (e.g., coal
41 combustion/biomass burning) to the rBC. Thus, the heavy pollution in Beijing was
42 greatly influenced by other sources in addition to the local traffic.

43 **Keywords:** black carbon aerosol, size distribution, source, haze

44

45 **1 Introduction**

46 Black carbon (BC), the major light-absorbing chemical component in atmospheric
47 aerosols, plays an important role in the radiative balance of the earth system through its
48 direct effect of heating the lower atmosphere and indirect effect of affecting cloud
49 properties (Ramanathan and Carmichael, 2008). Although BC is hydrophobic, it can
50 still act as cloud condensation nucleus when internally mixed with hydrophilic
51 chemical compounds (Zhang et al., 2008a), and thus indirectly affect cloud properties
52 and associated radiative budget (Ramanathan et al., 2001). BC aerosols thus have a
53 great impact on regional and global climate and weather (Menon et al., 2002;
54 Ramanathan and Carmichael, 2008; Ding et al., 2013; Liao et al., 2015; Huang et al.,
55 2016). BC can also increase atmospheric stability by its heating effect in the lower
56 troposphere and cooling role at the surface (Wang et al., 2013), which in turn suppresses
57 the diffusion of pollutants, deteriorates air quality, and enhances haze weather intensity
58 (Ding et al., 2016). However, quantifying BC's impact on radiative forcing and
59 environment is challenging and has large uncertainties because of the large variations
60 in its concentration and physicochemical properties (IPCC, 2013). The light absorption
61 of BC highly depends on its size distribution and morphology. Mie calculations for
62 hypothetical BC spheres show that the mass absorption cross-sections reach their peaks
63 at a diameter of ~150 nm and then decrease sharply with further increases in size (see
64 Fig. 4 in Bond and Bergstrom, 2006). However, atmospheric BC particles apparently
65 consist of aggregates of small primary spherules ~15 to 60 nm in diameter (Alexander
66 et al., 2008; Zhang et al., 2008a). They are chain agglomerates when freshly emitted
67 from the combustion sources resulting in increasing mass normalized absorption with
68 the particle mobility size (Khalizov et al., 2009). These fresh BC particles are quickly
69 coated by other aerosol components in the atmosphere, leading to the collapse of the
70 chain agglomerates into more compact BC cores (Zhang et al., 2008a). An alteration in
71 the morphology of BC due to a thin coating causes competition between light
72 absorption enhancement and decline, resulting in little variation in the absorption
73 efficiency (Wang et al., 2013; Peng et al., 2016). Subsequently, the thickened coating
74 of the scattering shell enwrapping the compact BC cores enhances the light absorption

75 of BC by the lensing effect, although the upper limit of the enhanced amplitude varied
76 among different studies (e.g., Schnaiter et al., 2005; Shiraiwa et al., 2010; Khalizov et
77 al., 2009; Peng et al., 2016).

78 With its rapid economic development, China has been suffering from heavy air
79 pollution (Yin and Wang, 2016). Annual BC emissions to the atmosphere in China are
80 very high, accounting for approximately half of the total emissions in Asia and one-
81 fifth globally (Qin and Xie, 2012). Existing studies on ambient BC mostly focused on
82 its mass concentrations (e.g., Cao et al., 2007; Zhang et al., 2008b), and little is known
83 about its physicochemical properties, including size, morphology, and mixing state (e.g.,
84 Huang and Yu, 2008; Cheng et al., 2012), mainly due to the limitations of the
85 measurement methodology. A traditional approach determining BC size distribution is
86 through analyzing the BC mass of size-segregated aerosol samples (Huang and Yu,
87 2008; Yu et al., 2010), which provides size information of BC-containing particles
88 because BC particles are frequently internally mixed with other aerosol components in
89 the atmosphere (Shiraiwa et al., 2007; Schwarz et al., 2008). The time resolution in this
90 approach was typically from hours to days. In the most recent decade, a novel analyzer,
91 single particle soot photometer (SP2), has been developed, which can measure mass
92 and size of the refractory BC (rBC) in high time resolution (Stephens et al., 2003;
93 Schwarz et al., 2006). The mixing state of rBC particles can also be derived from the
94 measurement of SP2 (Gao et al., 2007; Moteki and Kondo, 2007, 2008; Laborde et al.,
95 2012). Measurements of the sizes and mixing states of rBC based on this technology
96 has been limited to a few regions in China (e.g., Huang et al., 2012; Wang et al., 2014a,
97 2015a; Wu et al., 2016; Gong et al., 2016), as the SP2 is very expensive and its
98 performance is limited (Gysel et al., 2012; Liggio et al., 2012). It should be noted that
99 the sizes of rBC reported by SP2 are generally mass-equivalent diameters rather than
100 mobility- or aerodynamic-based ones, which are determined on the basis of the mass
101 measurements of individual rBC-containing particles. Thus, they are independent of the
102 morphology or mixing.

103 Although the physicochemical properties of BC in the atmosphere are greatly
104 diverse, its mass-equivalent sizes should vary little during their typical lifetime in the

105 atmosphere (~1 week) since BC itself is chemically inert under ambient conditions. In
106 other words, the mass-size of a BC particle is independent of its morphology and mixing
107 state, although coating with other components will reduce its mobility diameter and
108 enlarge the size of the mixed particle in which the BC is embedded. As it is a byproduct
109 of the incomplete combustion of fossil fuels and biomass, the BC size should be highly
110 dependent on the emission sources, including fuel type and combustion condition.
111 Based on the measurement of SP2, Liu et al. (2014) showed smaller sizes of the rBC
112 cores from traffic than those from solid fuel sources and attributed the rBC
113 concentrations from the two dominant sources accordingly. The rBC sizes measured at
114 rural or remote sites were considerably larger than those measured at urban sites (Huang
115 et al., 2012; Schwarz et al., 2013), implying that smaller sizes of rBC are emitted from
116 traffic sources. Combining the measurement of SP2 and the chemical source
117 apportionment of daily PM_{2.5} samples, Wang et al. (2016) showed that the rBC from
118 biomass burning and coal combustion had larger mass-equivalent diameter than that
119 from traffic.

120 Influenced by the local emissions (e.g., traffic exhaust) as well as regional
121 transport of air pollutants from the surrounding heavily polluted areas, the
122 physicochemical properties of ambient BC aerosols in urban Beijing are highly varied.
123 In this study, the mass-equivalent size distributions of rBC were first revealed in urban
124 Beijing based on the SP2 measurement during a wintertime in 2014 when haze occurred
125 frequently. The variations in the rBC size were also investigated, accompanied by an
126 analysis of its relation with aerosol chemical composition and its potential source
127 contributions. In the present study, a novel approach was employed to evaluate the
128 contribution of local traffic to the rBC concentration based on the measured rBC sizes
129 and reasonable assumptions including a deductive mean diameter of rBC from local
130 traffic and relatively stable rBC sizes in the air masses transported over certain regions.

131

132 **2 Methodology**

133 In situ measurements of rBC were conducted using a SP2 (Droplet Measurement
134 Technology, Inc., Boulder, CO, USA) on the rooftop (approximately 8 m above ground

135 level) of an experimental building at the Tower Division of the Institute of Atmospheric
136 Physics, Chinese Academy of Sciences (39°58'N, 116°22'E), during a late winter
137 period from 24 February to 15 March 2014 before the residential heating season ended.
138 The SP2 directly detects the incandescent intensity of an individual rBC-containing
139 particle when it passes through an intra-cavity Nd:YAG laser beam with a Gaussian
140 distribution (Schwarz et al., 2006). The incandescent intensity is converted to the mass
141 of rBC based on the calibration of incandescent signals of size-selected soot standards
142 performed pre/post-sampling. In this study, the Aquadag (Acheson, Inc., USA) was
143 used as a reference rBC and size-selected by a scanning mobility particle sizer
144 spectrometer (SMPS; TSI, Inc., Shoreview, MN, USA) for calibration. Compared to the
145 ambient rBC, it is more sensitive to the incandescence signal. Thus, a scaling factor of
146 0.75 is employed with the calibration curve to induce more reliable rBC mass
147 determinations (Baumgardner et al., 2012; Laborde et al., 2012). Moreover, an
148 approximately 10% underestimation of the SP2-derived bulk rBC mass concentration
149 due to the detection limitations outside the rBC mass range of ~0.3–120 fg was
150 considered (Wang et al., 2014a, 2015a). The total uncertainty in the rBC mass
151 determination was ~25%, including the uncertainties inherent in the mass calibration,
152 flow measurement and estimation of BC masses beyond the SP2 detection range (Wu
153 et al., 2016). The scattering signal is synchronously detected by the SP2 and used to
154 determine the optical size of a single particle (Gao et al., 2007; Laborde et al., 2012).
155 In this study, the scattering signal was employed to distinguish the mixing state of rBC-
156 containing particles. A traditional method based on the delay time between the
157 incandescent and scattering peaks was utilized to distinguish the rBC cores with and
158 without a thick coating (Schwarz et al., 2006; Moteki and Kondo, 2007; Wang et al.,
159 2014a; Wu et al., 2016). The rBC-containing particles were defined as either thickly
160 coated or uncoated/thinly coated according to the distribution of detected lag times,
161 which was bimodal and had a local minimum at 2 μ s (Fig. S1 in the supplemental files).
162 We defined the rBC particles as thickly coated if the lag times were longer than 2 μ s.
163 On this basis, the number fraction of thickly coated rBC (NF_{coated}), defined as the ratio
164 of the number of thickly-coated rBC particles to that of all detectable rBC particles, was

165 calculated to characterize the relative mixing extent of the BC aerosols in different
166 ambient samples. A similar measurement was conducted in January 2013, and more
167 details of the experimental setup and data process can be found in Wu et al. (2016).

168 Samples of PM_{2.5} were collected twice a day during this campaign, each lasting
169 for twelve hours. The chemical contents including organic carbon (OC), elemental
170 carbon (EC), water-soluble ions (e.g., SO₄²⁻, NO₃⁻, and NH₄⁺) and trace elements were
171 analyzed in the laboratory, as presented in detail by Lin et al. (2016).

172

173 **3 Results and Discussion**

174 **3.1 Size distribution of rBC and its variation**

175 As shown in Fig. 1, the mass of rBC ($dM/d\log D_p$) exhibited an approximately
176 lognormal distribution as a function of the volume-equivalent diameter (*VED*) of void-
177 free rBC, as has been commonly observed (e.g., Schwarz et al., 2006; Huang et al.,
178 2012; Wang et al., 2016). The similar size distribution was also observed in our previous
179 campaign in January 2013 (Fig. S2 in the supplemental files). A minor mode was also
180 captured at large sizes (peaked at ~600 nm), only accounting for ~6% of the SP2-
181 determined rBC masses. An analogous minor mode was previously observed at other
182 sites in China. Huang et al. (2011) reported a minor peak with a diameter of ~690 nm
183 at Kaiping, a rural site in the Pearl River Delta (PRD) region of China. Wang et al.
184 (2014b) found a minor peak with a diameter of ~470–500 nm in a remote area of the
185 Qinghai–Tibetan Plateau and considered it a likely feature of the rBC distribution of
186 biofuel/open fire burning sources, which needs further verification using measurements
187 of the size distributions at the emission sources. The peak diameter of the primary mode,
188 with a value of 213 nm, during the campaign is well within the range (~150–230 nm)
189 presented by previous studies conducted in different regions (Huang et al., 2012 and
190 references therein). It should be noted that the density of the assumed void-free rBC
191 was set to 1.8 g cm⁻³ in calculating the *VED* from the rBC masses measured in this
192 study, which should result in larger *VED* values compared to those based on the density
193 of 2.0 g cm⁻³ used in previous studies. If the density of 2.0 g cm⁻³ was employed, the
194 peak diameter of the primary mode would be ~206 nm in this study. This value is very

195 close to those observed in urban areas throughout China, e.g., 210 nm in Shenzhen in
196 South China (Huang et al., 2012), 205 nm in Xi'an in West China (Wang et al., 2015b),
197 and ~200 nm in Shanghai in East China (Gong et al., 2016). The relatively similar mass-
198 size distributions of rBC suggest that there were similar dominant emission sources in
199 different urban regions in China, where vehicle exhaust was one of the important
200 sources emitting rBC particles. Compared to those measured at rural sites in the PRD
201 region in South China (e.g., 220–222 nm, Huang et al., 2011, 2012), the peak diameters
202 of rBC in urban areas are significantly smaller. This might be related to the greater
203 amounts of coal combustion and biomass burning around the rural sites (Huang et al.,
204 2012). In contrast, the sizes of the rBC were much smaller in remote regions, e.g., with
205 a peak diameter of ~175–188 nm in the Qinghai–Tibetan Plateau area (Wang et al.,
206 2014b, 2015a). Wang et al. (2015a) attributed this smaller peak diameter value to the
207 source and considered that biomass burning generated a small rBC with peak *VED*
208 values in the range of ~187–193 nm. Another important reason for the smaller rBC
209 measured in remote regions, in our opinion, is that more large rBC particles are
210 deposited during their long-range transport to the observation site. Further research on
211 the sizes of rBC from different sources is needed.

212 The mass-size distributions of rBC during a polluted day (25 February) and a clean
213 one (4 March) are also compared in Fig. 1. The average mass concentrations of rBC
214 (MC_{rBC}) were $7.6 \mu\text{g m}^{-3}$ and $0.4 \mu\text{g m}^{-3}$, respectively, on the polluted and clean days.
215 The size distribution of rBC during the polluted day is similar to that during the entire
216 observation period, although a larger peak diameter was observed, with a value of 221
217 nm. In contrast, the peak diameter on the clean day is obviously smaller, with a value
218 of 199 nm. The secondary mode cannot be well characterized on the clean day. As
219 mentioned above, the mass-sizes of rBC emitted from a certain source change little
220 during their lifetime in the atmosphere. Thus, the considerable discrepancy of the rBC
221 sizes illustrates significant source alteration during the polluted period compared to that
222 on a clean day. Sun et al. (2014) used the measurements of ACSM at an urban site in
223 Beijing to show that the regional contribution to the BC exceeded 50% during heavily
224 polluted periods in January 2013. Model simulation also revealed that regional transport

225 contributed an average of 56% to the PM_{2.5} in Beijing in January 2013 when the hazes
226 occurred frequently, and even higher during polluted periods (Li and Han, 2016).
227 Accordingly, regional transport might play an important role in the increase in rBC
228 sizes during polluted periods in urban Beijing. By comparison, traffic emissions should
229 be the dominant source of rBC on the clean day, contributing to smaller rBC sizes.

230 The variation in the VED of the rBC is further investigated by comparing the mean
231 VED value of rBC (VED_{rBC}) with the mass ratios of secondary inorganic components
232 (i.e., ammonium sulfate, AS; ammonium nitrite, AN) to EC, a representation of the
233 aerosol aging degree. Generally, the average VED_{rBC} positively correlated with AS/EC
234 and AN/EC ratios with correlation coefficients of 0.63 ($p < 0.01$) and 0.61 ($p < 0.01$),
235 respectively (Fig. 2a and 2b). Higher AS/EC and AN/EC ratios were observed in
236 polluted samples, corresponding to higher VED_{rBC} during these periods.

237 It is interesting to note that the VED_{rBC} correlated more closely with AS/EC ratio
238 than AN/EC, especially under a clean condition. The correlation coefficient between
239 VED_{rBC} and AS/EC is 0.88 ($p < 0.01$) during clean periods with PM_{2.5} mass
240 concentrations lower than 35 $\mu\text{g m}^{-3}$ (blue dots in Fig. 2), much higher than that between
241 VED_{rBC} and AN/EC. By contrast, the NF_{coated} varied less with AS/EC during these
242 periods (Fig. 2c). This means that a higher AS/EC had less effect on the fraction of
243 thickly coated rBC during these clean periods but was related to larger rBC sizes, which
244 were highly dependent on the emission sources. In other words, higher AS/EC values
245 might indicate an increasing contribution of sources producing larger rBC other than
246 traffic, as sulfur is one of the major trace elements of coal combustion but not of traffic
247 (Zhang et al., 2013; Wang et al., 2016). On the other hand, NF_{coated} was highly related
248 to AN/EC, with a correlation coefficient of 0.81 ($p < 0.01$) during the clean periods (Fig.
249 2d). Even considering the entire samples, the correlation coefficient between NF_{coated}
250 and AN/EC was as high as 0.81 ($p < 0.01$), much higher than that (0.65, $p < 0.01$) between
251 NF_{coated} and AS/EC. This implies that the mixing state of rBC is much sensitive to
252 AN/EC in urban Beijing, especially during the clean periods. The secondary formation
253 of AN might play an important role in the coating processes of rBC but have a negligible
254 effect on the core size of the rBC.

255

256 **3.2 Potential source contribution to rBC mass and size**

257 The potential source contribution function (PSCF) analysis based on hourly
258 resolved 48-h backward trajectories arriving at the observation site 100 m above ground
259 level was performed using TrajStat software (Wang et al., 2009). The threshold of the
260 PSCF analysis was set to the mean value of each variable. A weight function on the
261 gridded PSCF values was employed on those cells having few trajectory endpoints
262 (Wang et al., 2006). Generally, the areas east and south of the observation site had the
263 largest number of potential source regions of high rBC concentrations, with weighted
264 PSCF (WPSCF) values of MC_{rBC} larger than 0.7 (Fig. 3a). Previous studies showed that
265 Hebei province, on the southern and eastern borders of Beijing, was a major contributor
266 to pollutants in Beijing, as its industrial activities are intense (Zhang et al., 2013). The
267 high coal consumption associated with the heavy industrial activities and residential
268 heating in the cold season should be an important source of high atmospheric rBC
269 loading in these areas. Similarly, the distribution of the WPSCF values of VED_{rBC} shows
270 that the eastern and southern regions are also correlated with large VED_{rBC} values (Fig.
271 3b). This implies that the pollution sources in these regions, e.g. heavy industrial
272 activities and residential heating, tend to produce highly concentrated rBC-containing
273 particles with large rBC core sizes. The source apportionment of rBC aerosols in
274 London based on in situ SP2 measurements showed that rBC-containing particles from
275 solid fuel sources (coal combustion and biomass burning) had significantly larger rBC
276 cores than those from traffic (Liu et al., 2014). Thus, the high WPSCF values of MC_{rBC}
277 and VED_{rBC} in the east and south might highly correlate to anthropogenic coal/biomass
278 combustion in these regions.

279 The spatial distribution of the WPSCF values of NF_{coated} is shown in Fig. 3c.
280 Associated with the aging processes that increase the thickly coating states of rBC-
281 containing particles through heterogeneous reactions, the WPSCF values of NF_{coated} are
282 generally high in the areas surrounding the observation site. It should be noted that
283 higher WPSCF values of NF_{coated} (> 0.7) dominate in the east to south. In addition to
284 the transport of thickly coated BC particles from these regions, aging processes of

285 locally emitted BC particles (e.g., from traffic sources) under the southerly winds
286 dominant condition, in which the relative humidity (RH) is high (Zhang et al., 2015;
287 Zheng et al., 2015), also increase the fraction of thickly coated rBC (Wu et al., 2016).
288 Although northerly/northwesterly winds also blow aged rBC-containing particles with
289 thick coatings, the larger amounts of non-/thinly coated BC particles from local sources
290 during these periods diminished the WPSCF values of NF_{coated} in the north to west
291 regions of the observation site. The low RH and strong winds from these directions are
292 unfavorable to the coating processes of locally emitted fresh rBC particles.

293 The VED_{coated} , defined as the VED of those thickly coated rBC cores, shows a
294 dispersive WPSCF distribution (Fig. 3d). Compared to the distribution of VED_{rBC} with
295 high WPSCF values that dominate in the east to south, high WPSCF values of VED_{coated}
296 are located in the northern pathway of air masses being transported to the observation
297 site as well. This implies that the regional transport of air masses brings large rBC, no
298 matter which direction it comes from. Dominated by the locally emitted small rBC, the
299 WPSCF values of VED_{rBC} are low in the northern region. It further illuminates that local
300 sources such as traffic emit small rBC, while regional transport brings in large rBC. On
301 the basis of the large discrepancy in rBC sizes between local traffic and regional
302 transport generated particles, it is possible to extract the contribution of local traffic
303 emissions from the mixed rBC sources.

304

305 **4 Discussion**

306 **4.1 Relationship between rBC size and mixing state**

307 As large rBC sizes are usually accompanied by significant contributions of
308 regional transport, which also lead to a high fraction of thickly coated rBC, the VED_{rBC}
309 is directly compared with the NF_{coated} as shown in Fig. 4. The two-dimensional
310 histogram of the 5-min average VED_{rBC} and NF_{coated} presents a significant linear
311 correlation between the two variables. It is characterized more clearly by the variation
312 in the mean VED_{rBC} values averaged in increased NF_{coated} bins with a resolution of 2%
313 (magenta circles in Fig. 4). The observed minimum value of the 5-min NF_{coated} is ~10%,
314 representing that there is little pure external mixing of rBC in the atmosphere, even for

315 short periods. However, an assumed mean VED of completely non/thinly coated rBC is
316 extrapolated from the linear curve to NF_{coated} with a value of 0% (i.e., the y-intercept
317 value). This inferred VED , with a value of ~ 150 nm, might be considered as the typical
318 mean VED of freshly emitted rBC from vehicle exhaust, which has little coating (Zhang
319 et al., 2008a; Peng et al., 2016). We are surprised to find that the linear relationship
320 between VED_{rBC} and NF_{coated} seems to be common, as was also found in another
321 campaign conducted in January 2013 (Wu et al., 2016) (gray circles in Fig. 4). More
322 observations are needed to further verify this relationship. According to the results
323 presented in this study, a mean VED of ~ 150 nm is legitimately accepted as the typical
324 SP2-determined mean VED of fresh rBC from local traffic sources. Size-segregated
325 aerosol samples also revealed a mode peaked at ~ 150 nm in aerodynamic diameter for
326 elemental carbon (EC) in urban Guangzhou, a megacity in PRD region, attributing to
327 the traffic emissions (Yu and Yu, 2009; Yu et al., 2010). A second mode at diameter of
328 ~ 400 nm was also observed and was also thought to be associated to the traffic emission
329 (Yu and Yu, 2009). In contrast, only the smaller EC mode with peak diameter in the
330 range of 100–200 nm was observed from traffic sources in urban areas of developed
331 counties (Allen et al., 2001; Kleeman et al., 2000). To date, no literature is available for
332 comparison with the case in Beijing because of the limitation in characterizing the size
333 distribution of EC at the small mode (e.g., < 400 nm). Considering the stringent fuel
334 and vehicle emission standards implemented in Beijing, the VED of ~ 150 nm for local
335 traffic source is reasonable, although further measurement studies are still needed to
336 verify this. As mentioned above, the VED of certain rBC varies little once it is emitted
337 to the atmosphere. Thus, the mean VED with a value of ~ 150 nm was employed in this
338 study as the representative of the rBC size from local traffic.

339 The variation in VED_{coated} with NF_{coated} is also shown (magenta triangles in Fig. 4).
340 It is interesting to find that, compared to VED_{rBC} , VED_{coated} presents a fluctuant
341 variation as NF_{coated} increases. The larger VED_{coated} at lower NF_{coated} is comprehensible
342 because regionally transported large rBC dominates in the thickly coated rBC particles,
343 and the small rBC from local traffic is mainly externally mixed with other aerosol
344 components at this stage. As the NF_{coated} increases from 10–20% to 30–40%, the mean

345 VED_{coated} gradually decreases from ~ 200 nm to ~ 190 nm. This implies that some small
346 rBC (e.g., rBC from local traffic) contributes a considerable portion of the thickly
347 coated rBC particles at this stage. In addition to the influence of the emission sources
348 on the rBC size, this decrease in VED_{coated} can also be explained by the contamination
349 of the local traffic emitted small rBC into the thickly coated rBC particles through
350 atmospheric aging processes (i.e., coating with other components). It should be noted
351 that the VED_{rBC} sustained increases at this stage, implying that other sources besides
352 the local traffic also brought large rBC at the same time. This is because if the increase
353 in NF_{coated} only results from the coating processes of the local traffic emitted rBC, the
354 VED of the entire rBC (i.e., VED_{rBC}) should vary little. The VED_{coated} increases
355 significantly when NF_{coated} exceeds 40%, suggesting that regional transport dominates
356 at this stage, bringing a large amount of thickly coated rBC particles with a large rBC
357 core. Meanwhile, the mean MC_{rBC} increases dramatically from $1.3 \mu\text{g m}^{-3}$ to $5.0 \mu\text{g m}^{-3}$
358 3 when NF_{coated} increases from 30% to 50%, further confirming the great contribution
359 of regional transport to the rBC at this stage. By comparison, the mean rBC
360 concentration varies in a small range of $0.8\text{--}1.4 \mu\text{g m}^{-3}$ when NF_{coated} is lower than 30%.
361 The observation from the campaign of 2013 showed a similar variation in VED_{coated}
362 against NF_{coated} (gray triangles in Fig. 4).

363

364 **4.2 Extracting the local traffic contribution to rBC**

365 As VED_{rBC} with a value of ~ 150 nm is expected to be the typical mean VED of the
366 local traffic emitted rBC and varies little in the atmosphere, it provides the possibility
367 of extracting the contribution of the local traffic to the rBC from the total rBC mass
368 concentration according to the variation in VED_{rBC} . However, the typical mean VED of
369 rBC from other sources, such as coal combustion and biomass burning, is difficult to
370 identify. It depends on many factors including fuel type and combustion condition. In
371 this study, a simple assumption was employed to identify the typical mean VED of rBC
372 from other sources besides local traffic according to where the air masses came from.
373 During a short period when the source emissions were relatively stable, the rBC from a
374 certain direction was assumed to have a certain mean VED , no matter from which

375 source it is emitted. Thus, a cluster analysis was performed on the 48-h backward
376 trajectories that arrived at the observation site. Five clusters were identified using
377 TrajStat software according to the total spatial variation in the cluster numbers (as
378 shown in Fig. S3). As the rBC tends to be thickly coated in the regionally transported
379 air masses, the mean VED of the rBC from sources other than local traffic was derived
380 from the values of VED_{coated} . The local traffic emitted small rBC can also become
381 thickly coated through aging processes in the atmosphere, so a further assumption is
382 employed to consider the VED of rBC from other sources equal to the mean value of
383 the upper 5% percentile of VED_{coated} in each cluster. Five typical mean VED s of rBC
384 from sources other than local traffic were identified, with values in the range of 195.5–
385 208.3 nm (Fig. S3). Such simple assumptions might induce large uncertainties in the
386 absolute contribution of the local traffic to the rBC, but it should well reflect the
387 variation in the traffic contribution.

388 Using a multiple linear regression to VED_{rBC} , the hourly-resolved traffic
389 contribution to the rBC was extracted on the basis of the derived VED of the rBC from
390 local traffic and other sources. The mass fraction of the traffic-induced rBC (MF_{traffic})
391 is shown in Fig. 5a (red line). During this campaign, approximately 35% to 100% of
392 the hourly MC_{rBC} is attributed to local traffic emissions, with a mean of 59%. Based on
393 a multiple linear regression analysis of the contributions of the three dominant factors
394 (i.e., traffic, coal combustion and biomass burning) to the rBC derived from the
395 chemical source apportionment of the daily $PM_{2.5}$ samples, Wang et al. (2016) showed
396 a slightly lower contribution of the traffic to the rBC in urban Xi'an, with a mean of
397 46% and a daily contribution in the range of 0.8 to 77.2%. Since entirely different
398 methods were employed in addition to the different locations, the resolved traffic
399 contribution to the rBC should not be compared absolutely. However, the relatively
400 lower MC_{rBC} in this study (with a mean of $2.8 \mu\text{g m}^{-3}$ compared to $8.0 \mu\text{g m}^{-3}$) might
401 partly interpret the slightly higher contribution of traffic, as a lower MC_{rBC} is usually
402 accompanied by a higher contribution of the local traffic. It is clear that MF_{traffic} is
403 negatively correlated with MC_{rBC} , with the correlation coefficient as high as -0.84
404 ($p < 0.01$) between the daily moving averaged MF_{traffic} and MC_{rBC} (Fig. 5a). This means

405 that the traffic contribution to the rBC decreased significantly during the polluted
406 periods when the rBC loading increased. In other words, the rBC from other sources
407 such as coal combustion and biomass burning played an increased role in these polluted
408 periods. This implies that the high MC_{rBC} in urban Beijing was not only due to the
409 accumulation of the local traffic emissions during stable synoptic conditions but also
410 attributed to the overlaying pollution from other sources.

411 The diurnal variations of the decomposed MC_{rBC} from local traffic and other
412 sources are shown in Fig. 5b and 5c, respectively. A common diurnal variation in MC_{rBC}
413 with high values during the nighttime and low ones in the daytime is shown for both
414 the traffic and other sources produced rBC, suggesting the important impact of the
415 mixing layer height on the surface MC_{rBC} . A high mixing layer in the daytime,
416 especially in the afternoon, favors the diffusion of the pollutants, leading to a low value
417 of MC_{rBC} . A low mixing layer in the nighttime suppresses the diffusion of pollutants,
418 resulting in a high value of MC_{rBC} . It is noted that a significant peak MC_{rBC} of local
419 traffic was observed in the early morning (05:00–06:00 local time). Moreover, the
420 increase in the local traffic related MC_{rBC} occurs earlier than that of other sources in the
421 evening. It corresponds well to the increased traffic contribution in the morning and
422 evening rush hours. Although the traffic flow showed a significant decrease in the
423 nighttime, a dramatic increase in the flow of heavy-duty diesel vehicles was observed
424 due to Beijing's traffic regulation (Song et al., 2013). These vehicles have much higher
425 emission factors of BC (~15–30 times) than light-duty gasoline ones, and thus play a
426 non-negligible role in the high MC_{rBC} values around midnight. Generally, the diurnal
427 variation of MC_{rBC} verifies to some degree the rationality of the method we employed
428 to distinguish the contribution of the local traffic emission from that of other sources.

429

430 **5 Summary and Concluding Remarks**

431 An approximate lognormal size distribution of the rBC in volume-equivalent
432 diameter was observed in urban Beijing during a polluted winter in 2014 based on
433 measurements using a SP2. The peak diameter was 213 nm, assuming void-free rBC
434 with a density of 1.8 g cm^{-3} , which is close to the values observed in other urban areas

435 in China. The measured sizes of the rBC were considerably larger during the polluted
436 period than clean period, implying a source variation of the rBC. The mean VED_{rBC}
437 positively correlated with the ratios of secondary inorganic aerosols (including AS and
438 AN) to EC, especially the ratio of AS/EC under a clean condition. This implies that the
439 rBC sizes are highly related to the emission sources because sulfur is one of the major
440 trace elements in coal combustion, while little is emitted from traffic. By comparison,
441 the mean NF_{coated} correlated more with AN/EC, implying the important effect of the
442 secondary formation of nitrate on the rBC mixing state. The PSCF analysis showed that
443 regional transport from the east to south of Beijing was a major source of high rBC
444 loading in Beijing and accompanied by a large VED_{rBC} and high NF_{coated} .

445 A significant positive correlation existed between VED_{rBC} and NF_{coated} , inferring
446 the typical mean VED of the rBC from local traffic, with a value of 150 nm. Based on
447 the inferred VED and further reasonable assumptions, the local traffic contribution to
448 the rBC was extracted. Local traffic emissions played an important role in the rBC
449 loading in urban Beijing and contributed 59% of the MC_{rBC} on campaign average.
450 However, its contribution decreased significantly in the polluted period compared to
451 the clean period. A significant negative correlation is found between the daily moving
452 average MC_{rBC} and MF_{traffic} with a coefficient of -0.87. A similar diurnal variation in
453 the decomposed MC_{rBC} associated with local traffic and other sources was observed
454 with high values in the nighttime and low in the daytime. However, a significant
455 increase in traffic MC_{rBC} was observed in the early morning and evening, indicating the
456 increased contribution of local traffic emissions. Despite potential large uncertainties
457 in the estimated contribution from the local traffic to rBC, due to the many assumptions
458 employed, its relative variation is clearly demonstrated. Further research measuring
459 sizes of rBC directly from various sources, including coal combustion, biomass burning
460 and traffic exhaust, is needed to validate the findings presented in this study. This work
461 provides a relatively simple but novel method to extract the contribution of the local
462 traffic to the rBC on the basis of the size measurement of the rBC in atmosphere, which
463 could enhance source apportionment research in urban Beijing and elsewhere air
464 pollution is severe.

465

466 **Acknowledgments:**

467 This work was supported by the National Natural Science Foundation of China (No.
468 91644217, 41575150 and 41305128), the Special Scientific Research Funds for
469 Environment Protection Commonweal Section (No. 201409027), and the Jiangsu
470 Collaborative Innovation Center for Climate Change.

471

472 **References:**

- 473 Alexander, D. T. L., Crozier, P. A., and Anderson, J. R.: Brown carbon spheres in East Asian outflow
474 and their optical properties, *Sciences*, 321, 833–836, 2008.
- 475 Allen, J. O., Mayo, P. R., Hughes, L. S., Salmon, L. G., and Cass, G. R.: Emissions of size-
476 segregated aerosols from on-road vehicles in the Caldecott Tunnel, *Environ. Sci. Technol.*, 35,
477 4189–4197, 2001.
- 478 Baumgardner, D., Popovicheva, O., Allan, J., Bernardoni, V., Cao, J., Cavalli, F., Cozic, J., Diapouli,
479 E., Eleftheiadis, K., Genberg, P. J., Gonzalez, C., Gysel, M., John, A., Kirchstetter, T. W.,
480 Kuhlbusch, T. A. J., Laborde, M., Lack, D., Müller, T., Niessner, R., Petzold, A., Piazzalunga,
481 A., Putaud, J. P., Schwarz, J., Sheridan, P., Surramanian, R., Swietlicki, E., Valli, G., Vecchi,
482 R., and Viana, M.: Soot reference materials for instrument calibration and intercomparisons: a
483 workshop summary with recommendations, *Atmos. Meas. Tech.*, 5, 1869–1887, 2012.
- 484 Bond, T. C., and Bergstrom, R. W.: Light absorption by carbonaceous particles: an investigative
485 review, *Aerosol Sci. Technol.*, 40, 27–67, 2006.
- 486 Cao, J. J., Lee, S. C., Chow, J. C., Watson, J. G., Ho, K. F., Zhang, R. J., Jin, Z. D., Shen, Z. X.,
487 Chen, G. C., Kang, Y. M., Zou, S. C., Zhang, L. Z., Qi, S. H., Dai, M. H., Cheng, Y., and Hu,
488 K.: Spatial and seasonal distributions of carbonaceous aerosols over China, *J. Geophys. Res.*,
489 112, D22S11, doi:10.1029/2006JD008205, 2007.
- 490 Cheng, Y. F., Su, H., Rose, D., Gunthe, S. S., Berghof, M., Wehner, B., Achtert, P., Nowak, A.,
491 Takegawa, N., Kondo, Y., Shiraiwa, M., Gong, Y. G., Shao, M., Hu, M., Zhu, T., Zhang, Y. H.,
492 Carmichael, G. R., Wiedensohler, A., Andreae, M. O., and Pöschl, U.: Size-resolved
493 measurement of the mixing state of soot in the megacity Beijing, China: diurnal cycle, aging
494 and parameterization, *Atmos. Chem. Phys.*, 12, 4477–4491, 2012.
- 495 Ding, A. J., Fu, C. B., Yang, X. Q., Sun, J. N., Petäjä, T., Kerminen, V., Wang, T., Xie, Y. N.,
496 Herrmann, E., Zheng, L., Nie, W., Liu, Q., Wei X., and Kulmala, M.: Intense atmospheric
497 pollution modifies weather: a case of mixed biomass burning with fossil fuel combustion
498 pollution in the eastern China, *Atmos. Chem. Phys.*, 13, 10545-10554, 2013.
- 499 Ding, A. J., Huang, X., Nie, W., Sun, J. N., Kerminen, V.-M., Petäjä, T., Su, H., Cheng, Y. F., Yang,
500 X.-Q., Wang, M. H., Chi, X. G., Wang, J. P., Virkkula, A., Guo, W. D., Yuan, J., Wang, S. Y.,
501 Zhang, R. J., Wu, Y. F., Song, Y., Zhu, T., Zilitinkevich, S., Kulmala, M., and Fu, C. B.:
502 Enhanced haze pollution by black carbon in megacities in China, *Geophys. Res. Lett.*, 43,
503 2873–2879, 2016.
- 504 Gao, R. S., Schwarz, J. P., Kelly, K. K., Fahey, D. W., Watts, L. A., Thompson, T. L., Spackman, J.
505 R., Slowik, J. G., Cross, E. S., Han, J.-H., Davidovits, P., Onasch, T. B., and Worsnop, D. R.:
506 A novel method for estimating light-scattering properties of soot aerosols using a modified
507 single-particle soot photometer, *Aerosol Sci. Technol.*, 41, 125–135, 2007.
- 508 Gong, X. D., Zhang, C., Chen, H., Nizkorodov, S. A., Chen, J. M., and Yang, X.: Size distribution
509 and mixing state of black carbon particles during a heavy air pollution episode in Shanghai,
510 *Atmos. Chem. Phys.*, 16, 5399–5411, 2016.
- 511 Gysel, M., Laborde, M., Mensah, A., Corbin, J., Keller, A., Kim, J., Petzold, A., and Sierau, B.:
512 Technical note: The single particle soot photometer fails to reliably detect PALAS soot
513 nanoparticles, *Atmos. Meas. Tech.*, 5, 3099–3107, 2012.
- 514 Huang, X., Ding, A. J., Liu, L. X., Liu, Q., Ding, K., Niu, X. R., Nie, W., Xu, Z., Chi, X. G., Wang,
515 M. H., Sun, J. N., Guo, W. D., and Fu, C. B.: Effects of aerosol-radiation interaction on

516 precipitation during biomass-burning season in East China, *Atmos. Chem. Phys.*, 16, 10063–
517 10082, 2016.

518 Huang, X. F., and Yu, J. Z.: Size distributions of elemental carbon in the atmosphere of a coastal
519 urban area in South China: characteristics, evolution processes, and implications for the mixing
520 state, *Atmos. Chem. Phys.*, 8, 5843–5853, 2008.

521 Huang, X. F., Gao, R. S., Schwarz, J. P., He, L. Y., Fahey, D. W., Watts, L. A., McComiskey, A.,
522 Cooper, O. R., Sun, T. L., Zeng, L. W., Hu, M., and Zhang, Y. H.: Black carbon measurements
523 in the Pearl River Delta region of China, *J. Geophys. Res.*, 116, D12208,
524 doi:10.1029/2010JD014933, 2011.

525 Huang, X. F., Sun, T. L., Zeng, L. W., Yu, G. H., and Luan, S. J.: Black carbon aerosol
526 characterization in a coastal city in South China using a single particle soot photometer, *Atmos.*
527 *Environ.*, 51, 21–28, 2012.

528 IPCC, 2013. Summary for policymakers. In: Stocker, T.F., Qin, D., Plattner, G.-K., Tignor, M., Allen,
529 S.K., Boschung, J., Nauels, A., Xia, Y., Bex, V., Midgley, P.M. (Eds.), *Climate Change 2013:*
530 *The Physical Science Basis. Contribution of Working Group I to the Fifth Assessment Report*
531 *of the Intergovernmental Panel on Climate Change.* Cambridge University Press, Cambridge,
532 United Kingdom and New York, NY, USA.

533 Khalizov, A. F., Xue, H. X., Wang, L., Zheng, J., and Zhang, R. Y.: Enhanced light absorption and
534 scattering by carbon soot aerosol internally mixed with sulfuric acid, *J. Phys. Chem. A*, 113,
535 1066–1074, 2009.

536 Kleeman, M.J., Schauer, J. J., and Cass, G. R.: Size and composition distribution of fine particulate
537 matter emitted from motor vehicles, *Environ. Sci. Technol.* 34(7), 1132–1142, 2000.

538 Laborde, M., Mertes, P., Zieger, P., Dommen, J., Baltensperger, U., and Gysel, M.: Sensitivity of the
539 single particle soot photometer to different black carbon types, *Atmos. Meas. Tech.*, 5, 1031–
540 1043, 2012.

541 Li, J. W., and Han, Z. W.: A modeling study of severe winter haze events in Beijing and its
542 neighboring regions, *Atmos. Res.*, 170, 87–97, 2016.

543 Liao, H., and Shang, J. J.: Regional warming by black carbon and tropospheric ozone: a review of
544 progresses and research challenges in China, *J. Meteor. Res.*, 29, 525–545, 2015.

545 Liggio, J. Gordon, M., Smallwood, G., Li, S.-M., Stroud, C., Staebler, R., Lu, G., Lee, P., Taylor,
546 B., and Brook, J. R.: Are emissions of black carbon from gasoline vehicles underestimated?
547 Insights from near and on-road measurements, *Environ. Sci. Technol.*, 46, 4819–4828, 2012.

548 Lin, Y.-C., Hsu, S.-C., Chou, C.-C.-K., Zhang, R. J., Wu, Y. F., Kao, S.-J., Luo, L., Huang, C.-H.,
549 Lin, S.-H., and Huang, Y.-T.: Wintertime haze deterioration in Beijing by industrial pollution
550 deduced from trace metal fingerprints and enhanced health risk by heavy metals, *Environ.*
551 *Pollut.*, 208, 284–293, 2016.

552 Liu, D., Allan, J. D., Young, D. E., Coe, H., Beddows, D., Fleming, Z. L., Flynn, M. J., Gallagher,
553 M. W., Harrison, R. M., Lee, J., Prevot, A. S. H., Taylor, J. W., Yin, J., Williams, P. I., and
554 Zotter, P.: Size distribution, mixing state and source apportionment of black carbon aerosol in
555 London during wintertime, *Atmos. Chem. Phys.*, 14, 10061–10084, 2014.

556 Menon, S., Hansen, J., Nazarenko, L., and Luo, Y. F.: Climate effects of black carbon aerosols in
557 China and India, *Science*, 297, 2250–2253, 2002.

558 Moteki, N., and Kondo, Y.: Effects of mixing state on black carbon measurements by laser-induced
559 incandescence, *Aerosol Sci. Technol.*, 41, 398–417, 2007.

560 Moteki, N., and Kondo, Y.: Method to measure time-dependent scattering cross sections of particles
561 evaporating in a laser beam, *J. Aerosol Sci.*, 39, 348–364, 2008.

562 Peng, J. F., Hu, M., Guo, S., Du, Z. F., Zheng, J., Shang, D. J., Zamora, M. L., Zeng, L. M., Shao,
563 M., Wu, Y.-S., Zheng, J., Wang, Y., Glen, C. R., Collins, D. R., Molina, M. J., and Zhang, R.
564 Y.: Markedly enhanced absorption and direct radiative forcing of black carbon under polluted
565 urban environments, *Proc. Natl. Acad. Sci. U.S.A.*, 113, 4266–4271, 2016.

566 Qin, Y., and Xie, S. D.: Spatial and temporal variation of anthropogenic black carbon emissions in
567 China for the period 1980–2009, *Atmos. Chem. Phys.*, 12, 4825–4841, 2012.

568 Ramanathan, V., Crutzen, P. J., Kiehl, J. T., and Rosenfeld, D.: Aerosols, climate, and the
569 hydrological cycle, *Science*, 294, 2119–2125, 2001.

570 Ramanathan, V., and Carmichael, G.: Global and regional climate changes due to black carbon,
571 *Nature Geosci.*, 1, 221–227, 2008.

572 Schnaiter, M., Linke, C., Möhler, O., Naumann, K. H., Saathoff, H., Wagner, R., Schurath, U., and
573 Wehner, B.: Absorption amplification of black carbon internally mixed with secondary organic
574 aerosol, *J. Geophys. Res.*, 110, D19204, doi:10.1029/2005JD006046, 2005.

575 Schwarz, J. P., Gao, R. S., Fahey, D. W., Thomson, D. S., Watts, L. A., Wilson, J. C., Reeves, J. M.,
576 Darbeheshti, M., Baumgardner, D. G., Kok, G. L., Chung, S. H., Schulz, M., Hendricks, J.,
577 Lauer, A., Kärcher, B., Slowik, J. G., Rosenlof, K. H., Thompson, T. L., Langford, A. Q.,
578 Loewenstein, M., and Aikin, K. C.: Single-particle measurements of midlatitude black carbon
579 and light-scattering aerosols from the boundary layer to the lower stratosphere, *J. Geophys.*
580 *Res.*, 111, D16207, doi:10.1029/2006JD007076, 2006.

581 Schwarz, J. P., Gao, R. S., Spackman, J. R., Watts, L. A., Thomson, D. S., Fahey, D. W., Ryerson,
582 T. B., Peischl, J., Holloway, J. S., Trainer, M., Frost, G. J., Baynard, T., Lack, D. A., de Gouw,
583 J. A., Warneke, C., and Del Negro, L. A.: Measurement of the mixing state, mass, and optical
584 size of individual black carbon particles in urban and biomass burning emissions, *Geophys.*
585 *Res. Lett.*, 35, L13810, doi:10.1029/2008GL033968, 2008.

586 Schwarz, J. P., Gao, R. S., Perring, A. E., Spackman, J. R., and Fahey, D. W.: Black carbon aerosol
587 size in snow, *Sci. Rep.*, 3, 1356, doi:10.1038/srep01356, 2013.

588 Shiraiwa, M., Kondo, Y., Moteki, N., Takegawa, N., Miyazaki, Y., and Blake, D. R.: Evolution of
589 mixing state of black carbon in polluted air from Tokyo, *Geophys. Res. Lett.*, 34, L16803,
590 doi:10.1029/2007GL029819, 2007.

591 Shiraiwa, M., Kondo, Y., Iwamoto, T., Kita, K.: Amplification of light absorption of black carbon by
592 organic coating, *Aerosol Sci. Technol.*, 44, 46–54, 2010.

593 Song, S., Wu, Y., Xu, J., Ohara, T., Hasegawa, S., Li, J., Yang, L., and Hao, J.: Black carbon at a
594 roadside site in Beijing: Temporal variations and relationships with carbon monoxide and
595 particle number size distribution, *Atmos. Environ.*, 77, 213–221, 2013.

596 Stephens, M., Turner, N., and Sandberg, J.: Particle identification by laser-induced incandescence
597 in a solid-state laser cavity, *Appl. Opt.*, 42, 3726–3736, 2003.

598 Sun, Y. L., Jiang, Q., Wang, Z. F., Fu, P. Q., Li, J., Yang, T., and Yin, Y.: Investigation of the sources
599 and evolution processes of severe haze pollution in Beijing in January 2013, *J. Geophys. Res.*
600 *Atmos.*, 119, 4380–4398, 2014.

601 Wang, Q. Y., Huang, R. J., Cao, J. J., Han, Y. M., Wang, G. H., Li, G. H., Wang, Y. C., Dai, W. T.,
602 Zhang, R. J., and Zhou, Y. Q.: Mixing state of black carbon aerosol in a heavily polluted urban
603 area of China: implications for light absorption enhancement, *Aerosol Sci. Technol.*, 48, 689–

604 697, 2014a.

605 Wang, Q. Y., Schwarz, J. P., Cao, J. J., Gao, R. S., Fahey, D. W., Hu, T. F., Huang, R. J., Han, Y. M.,
606 and Shen, Z. X.: Black carbon aerosol characterization in a remote area of Qinghai–Tibetan
607 Plateau, western China, *Sci. Total Environ.*, 479–480, 151–158, 2014b.

608 Wang, Q. Y., Huang, R. J., Cao, J. J., Tie, X. X., Ni, H. Y., Zhou, Y. Q., Han, Y. M., Hu, T. F., Zhu,
609 C. S., Feng, T., Li, N., and Li, J. D.: Black carbon aerosol in winter northeastern Qinghai–
610 Tibetan Plateau, China: the source, mixing state and optical property, *Atmos. Chem. Phys.*, 15,
611 13059–13069, 2015a.

612 Wang, Q. Y., Liu, S. X., Zhou, Y. Q., Cao, J. J., Han, Y. M., Ni, H. Y., Zhang, N. N., and Huang, R.
613 J.: Characteristics of Black Carbon Aerosol during the Chinese Lunar Year and Weekdays in
614 Xi’an, China, *Atmosphere*, 6, 195–208, 2015b.

615 Wang, Q. Y., Huang, R. J., Zhao, Z. Z., Cao, J. J., Ni, H. Y., Tie, X. X., Zhao, S. Y., Su, X. L., Han,
616 Y. M., Shen, Z. X., Wang, Y. C., Zhang, N. N., Zhou, Y. Q., and Corbin, J. C.: Physicochemical
617 characteristics of black carbon aerosol and its radiative impact in a polluted urban area of China,
618 *J. Geophys. Res. Atmos.*, 121, doi:10.1002/2016JD024748, 2016.

619 Wang, Y., Khalizov, A., Levy, M., and Zhang, R. Y.: New direction: light absorbing aerosols and
620 their atmospheric impacts, *Atmos. Environ.*, 81, 713–715, 2013.

621 Wang, Y. Q., Zhang, X. Y., and Arimoto, R.: The contribution from distant dust sources to the
622 atmospheric particulate matter loadings at Xi’an, China during spring, *Sci. Total Environ.*, 368,
623 875–883, 2006.

624 Wang, Y. Q., Zhang, X. Y., and Draxler, R. R.: TrajStat: GIS-based software that uses various
625 trajectory statistical analysis methods to identify potential sources from long-term air pollution
626 measurement data, *Environ. Modell. Softw.*, 24, 938–939, 2009.

627 Wu, Y. F., Zhang, R. J., Tian, P., Tao, J., Hsu, S.-C., Yan, P., Wang, Q. Y., Cao, J. J., Zhang, X. L.,
628 and Xia, X. A.: Effect of ambient humidity on the light absorption amplification of black
629 carbon in Beijing during January 2013, *Atmos. Environ.*, 124, 217–223, 2016.

630 Yin, Z. C., and Wang, H. J.: Seasonal prediction of winter haze days in the north central North China
631 Plain, *Atmos. Chem. Phys.*, 16, 14843–14852, 2016.

632 Yu, H., and Yu, J. Z.: Modal characteristics of elemental and organic carbon in an urban location in
633 Guangzhou, China, *Aerosol Sci. Technol.*, 43, 1108–1118, 2009.

634 Yu, H., Wu, C., Wu, D., and Yu, J. Z.: Size distributions of elemental carbon and its contribution to
635 light extinction in urban and rural locations in the Pearl River Delta region, China, *Atmos.*
636 *Chem. Phys.*, 10, 5107–5119, 2010.

637 Zhang, Q., Quan, J. N., Tie, X. X., Li, X., Liu, Q., Gao, Y., and Zhao, D. L.: Effects of meteorology
638 and secondary particle formation on visibility during heavy haze events in Beijing, China, *Sci.*
639 *Total Environ.*, 502, 578–584, 2015.

640 Zhang, R., Jing, J., Tao, J., Hsu, S.-C., Wang, G., Cao, J., Lee, C.S.L., Zhu, L., Chen, Z., Zhao, Y.,
641 and Shen, Z.: Chemical characterization and source apportionment of PM_{2.5} in Beijing:
642 seasonal perspective, *Atmos. Chem. Phys.*, 13, 7053–7074, 2013.

643 Zhang, R. Y., Khalizov, A. F., Pagels, J. Zhang, D., Xue, H. X., and McMurry, P. H.: Variability in
644 morphology, hygroscopicity, and optical properties of soot aerosols during atmospheric
645 processing, *Proc. Natl. Acad. Sci. U.S.A.*, 105, 10291–10296, 2008a.

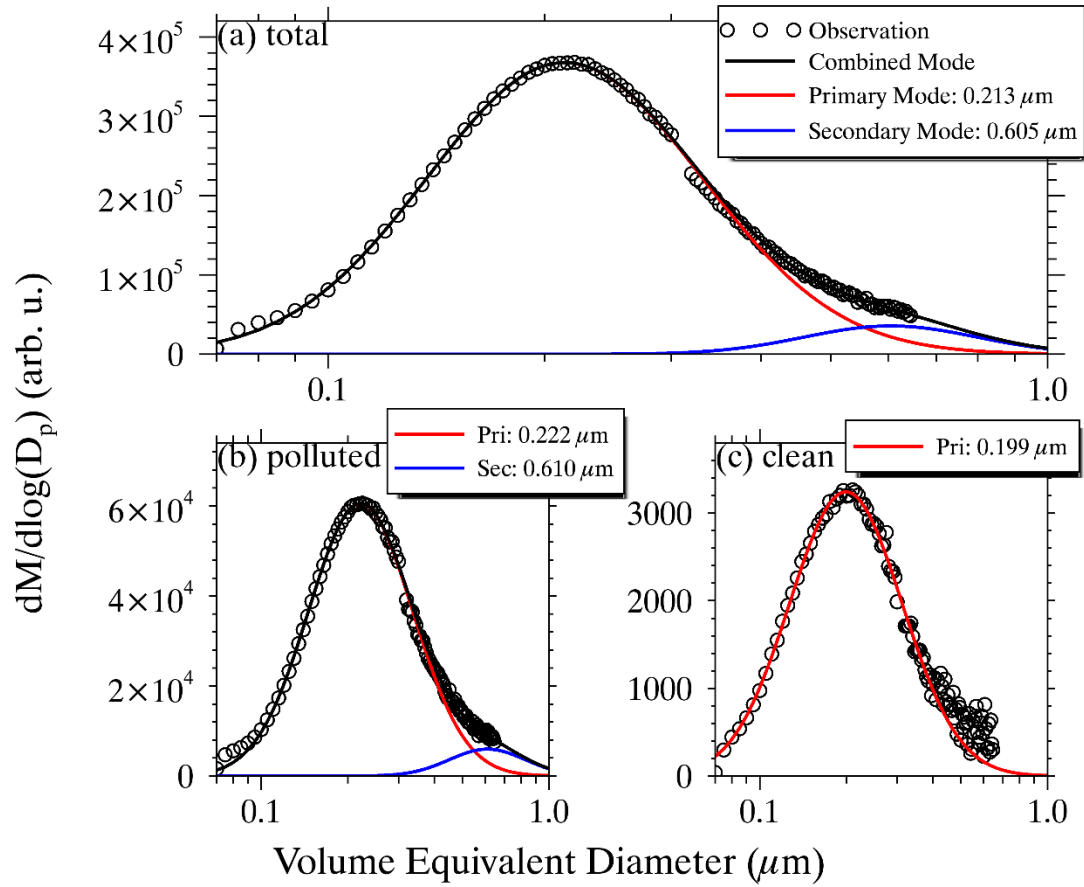
646 Zhang, X. Y., Wang, Y. Q., Zhang, X., Guo, W., Gong, S. L.: Carbonaceous aerosol composition
647 over various regions of China during 2006, *J. Geophys. Res.*, 113, D14111,

648 doi:10.1029/2007JD009525, 2008b.

649 Zheng, G. J., Duan, F. K., Su, H., Ma, Y. L., Cheng, Y., Zheng, B., Zhang, Q., Huang, T., Kimoto,
650 T., Chang, D., Pöschl, U., Cheng, Y. F., and He, K. B.: Exploring the severe winter haze in
651 Beijing: the impact of synoptic weather, regional transport and heterogeneous reactions, *Atmos.*
652 *Chem. Phys.*, 15, 2969–2983, 2015.

653

654



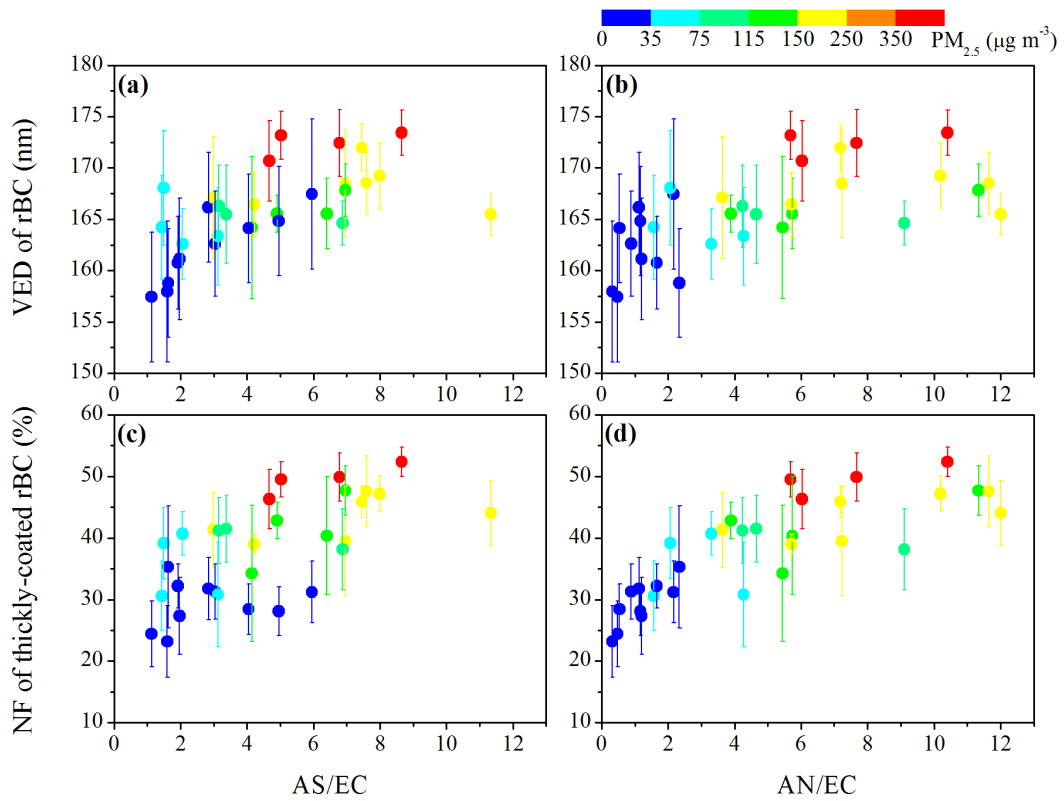
655

656 Fig. 1. Size distributions of rBC in volume-equivalent diameter during a campaign from 24 February

657 to 15 March, 2014. The red and blue lines are the lognormal fittings to the primary and secondary

658 modes, respectively, and the black ones correspond to the combined mode.

659



660

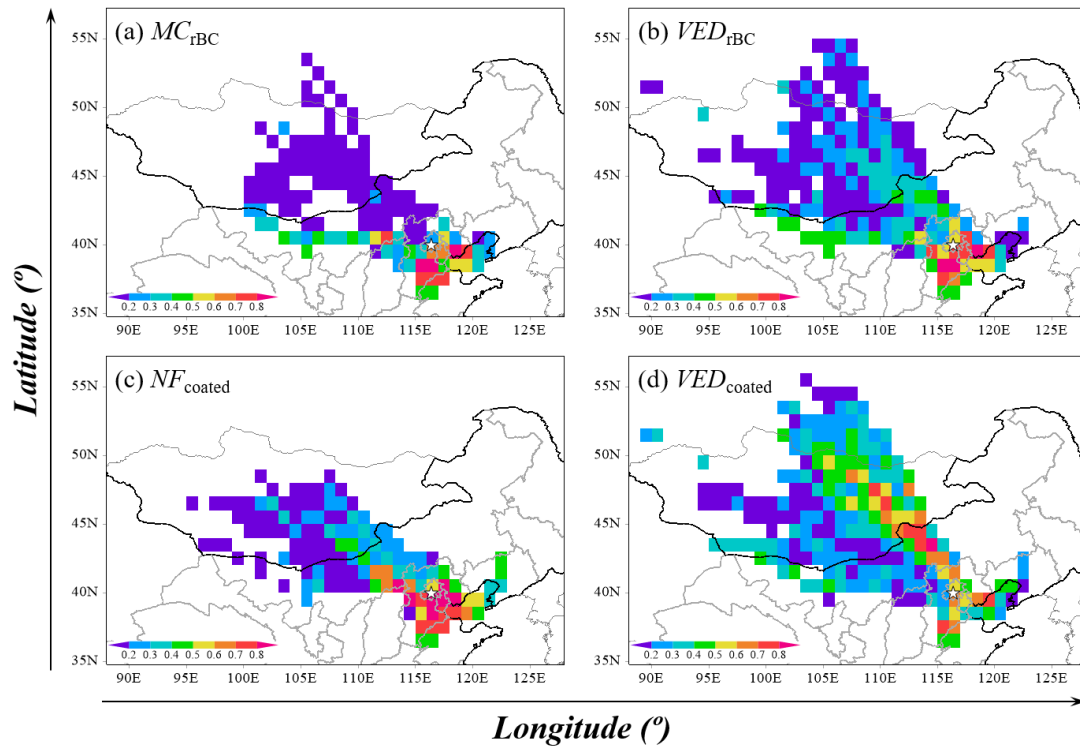
661 Fig. 2. Variation in the average volume-equivalent diameters of rBC (VED_{rBC}) as a function of the
 662 mass ratios of (a) ammonium sulfate (AS) and (b) ammonium nitrite (AN) to elemental carbon (EC).

663 The same apply for (c) and (d), but for the number fraction of thickly coated rBC (NF_{coated}). The

664 vertical bar denotes one standard deviation. The color scale represents the pollution levels defined

665 as the PM_{2.5} mass concentration according to the AQI standard of MEP of China.

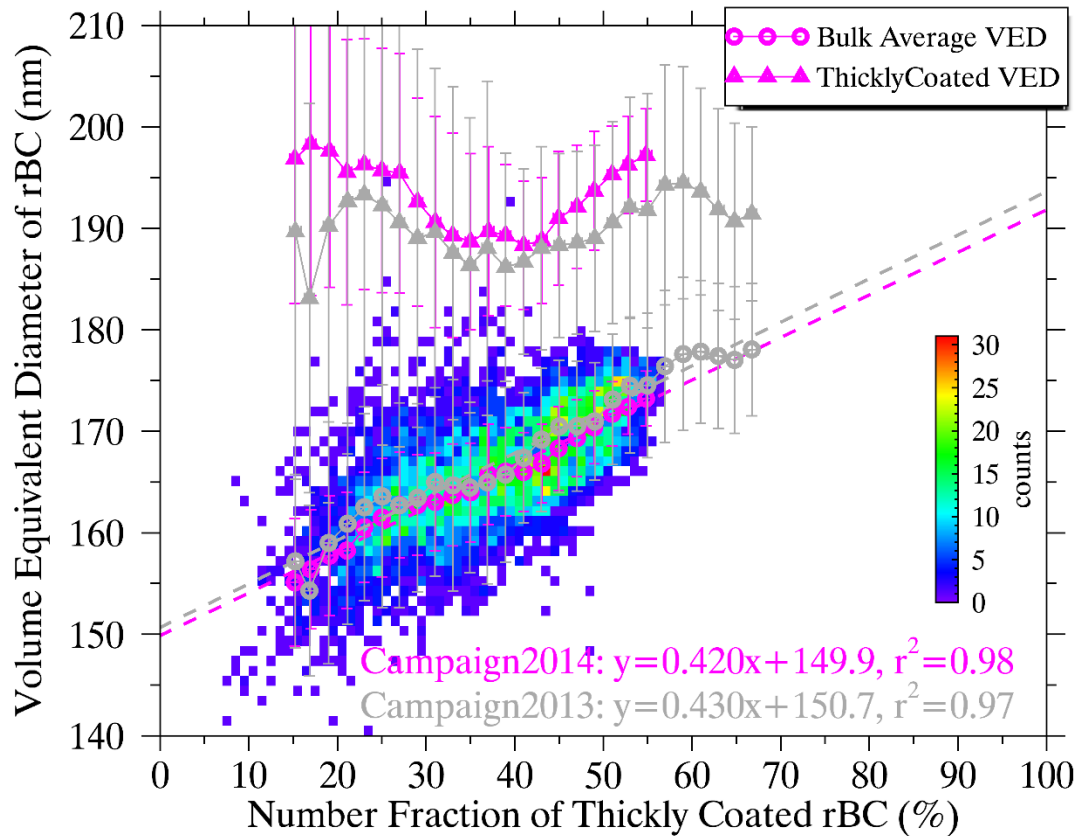
666



667

668 Fig. 3. Distributions of gridded ($1^\circ \times 1^\circ$) potential source contribution functions of (a) mass
 669 concentration (MC) and (b) volume equivalent diameter (VED) of rBC, and (c) number fraction (NF)
 670 and (d) VED of thickly coated rBC. The overlaid star symbol represents the geographical location
 671 of the observation site.

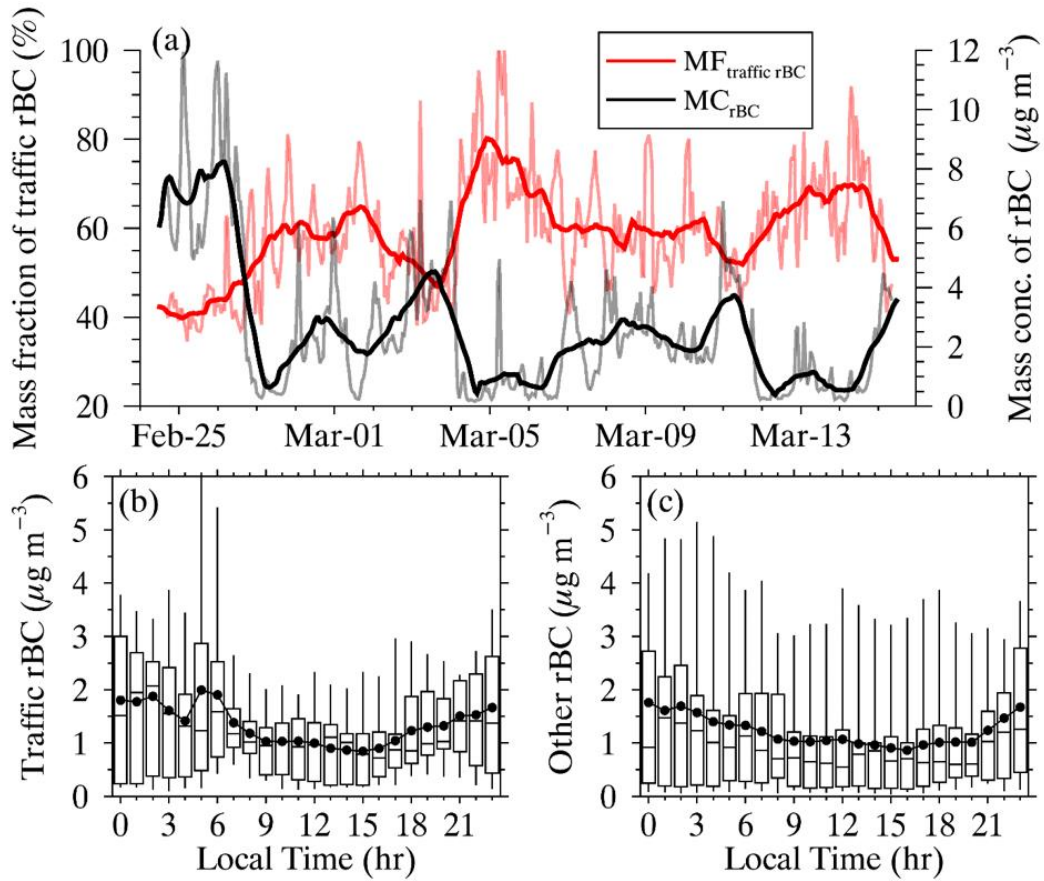
672



673

674 Fig. 4. Two-dimensional histogram of the 5-min average volume equivalent diameter of rBC
 675 (VED_{rBC}) against number fraction of thickly coated rBC (NF_{coated}) during the campaign in the late
 676 winter in 2014. The magenta circles and triangles with error bars represent the mean VED_{rBC} and
 677 VED of thickly-coated rBC (VED_{coated}) averaged in each NF_{coated} bin with a resolution of 2%,
 678 respectively. The dashed magenta line denotes the linear regression of VED_{rBC} against NF_{coated} . The
 679 relationship between VED_{rBC} and NF_{coated} during another campaign in January 2013 (Wu et al., 2016)
 680 is comparatively overlapped in gray.

681



682

683 Fig. 5. (a) Time series of hourly mass concentration of rBC (MC_{rBC}) and mass fraction of local traffic
 684 related rBC (MF_{traffic}). The bold lines represent the variations of the daily moving averaged MC_{rBC}
 685 and MF_{traffic} . (b) and (c) show the diurnal variations in the decomposed rBC from local traffic
 686 emission and other sources, respectively.